

Inconsistency between the Stokes-Einstein relation and its variants in supercooled water

Gan Ren¹, Yanting Wang^{2,3,*}

¹Department of Physics, Civil Aviation Flight University of China, Guanghan 628307, China

²CAS Key Laboratory of Theoretical Physics, Institute of Theoretical Physics, Chinese Academy of Sciences, Beijing 100190, China. E-mail: wangyt@itp.ac.cn

³School of Physical Sciences, University of Chinese Academy of Sciences, Beijing 100049, China

Abstract

The Stokes-Einstein (SE) relation $D = k_B T / C \eta a$ has three commonly used variants: $D \sim \tau^{-1}$, $D \sim T/\tau$ and $D \sim T/\eta$. In this work, the consistency of the original SE relation and its three variants in supercooled water is examined by molecular dynamics simulation with the TIP5P and Jagla water models, respectively. It is found that the original SE relation remains valid even when the three variants are all invalid in the simulated temperature ranges: $D \sim \tau^{-1}$ and $D \sim T/\tau$ follow the fractional forms $D \sim \tau^{-\xi}$ and $D \sim (\tau/T)^{-\xi}$ with a crossover temperature, at which the wavevector-dependent exponent ξ changes its value; $D \sim T/\eta$ is equivalent to the original SE relation only when the effective hydrodynamic radius a is a constant, which is however found to decrease with decreasing temperature T . Therefore, care should be taken when employing its variants to judge the validity of the original SE relation in supercooled water.

1. Introduction

The Stokes-Einstein (SE) relation (I) relates the diffusion constant D and the frictional coefficient α of particles moving in a viscous fluid, namely $D = k_B T / \alpha$, where k_B is the Boltzmann constant, T is

the temperature, $\alpha = C\eta a$ with η being the shear viscosity, a being the effective hydrodynamic radius, and C being a constant depending on the boundary condition. The SE relation has been successfully applied to many cases, such as the diffusion of protein (2), the effective molecular hydrodynamic radius in solutions (3), oxygen transport in cells (4), rheological properties of lubricant components (5), colloids (6, 7), solutions and pure liquids (8-14). On the other hand, the breakdown of the SE relation is commonly regarded as the appearance of a glassy state and/or anomalous behaviors. Particularly, the SE relation is observed to be breakdown in water (15-19) and other uniform liquids (20-22) when they undergo supercooling. Nevertheless, instead of its original form, the validity of the SE relation is quite often tested by its three variants, $D \sim T/\eta$ (17, 18, 23-25), $D \sim \tau^{-1}$ (22, 26-31), and $D \sim T/\tau$ (15, 16, 32, 33), with τ the structural relaxation time. The expression $D \sim T/\eta$ becomes a substitute of $D = k_B T / C\eta a$ by assuming that the effective hydrodynamic radius a is a constant in uniform liquids (17, 32). Due to the difficulty of accurately determining η in molecular dynamics (MD) simulation, τ is frequently adopted to replace η , under the condition that the temperature dependence of τ is similar to that of η (or η/T) (15, 32). The variant $D \sim \tau^{-1}$ results from the assumption that the particle displacement follows Gaussian (34). It is also an approximation in the mode coupling theory when the temperature is closed to the glass phase transition point (22, 34). Finally, the variant $D \sim T/\tau$ comes from the approximate relation $\eta = G_\infty \tau$ (15, 33, 35), where G_∞ is the instantaneous shear modulus presumed to be a constant.

The variant $D \sim T/\eta$ has been experimentally observed (18, 24) to be invalid for supercooled water: $D\eta/T$ is initially a constant during cooling and then starts to increase when T is below a certain value, which follows a fractional form $D \sim (T/\eta)^\xi$ with the exponent $\xi \neq 1$; the breakdown of $D \sim T/\eta$ has been proposed to result from the spatially heterogeneous dynamics and collective motions. Similar results were also observed in the simulations of the supercooled water with the TIP4P/2005 (17, 36, 37) and SPC/E water models (23). Kawasaki and Kang (17) have observed that $D \sim T/\eta$ is valid above a

crossover temperature T_x but follows a fractional form when $T < T_x$, which has been attributed to the increasing solidity upon supercooling. Chen and coworkers (19) have observed the breakdown of the variants $D \sim \tau^{-1}$ and $D \sim T/\tau$ in confined supercooled water, which has been attributed to the dynamic crossover caused by the change of the hydrogen-bond structure. Mallamace and coworkers (26, 38) have also observed similar phenomena in supercooled water confined in a nanotube. Kumar and coworkers (33) have observed that $D\tau/T$ in the MD simulations of water modeled by TIP5P and ST2, respectively, is not a constant as temperature decreases, and they propose that the breakdown is located at the point crossing the Widom line associated with the liquid-liquid phase transition. Based on both experimental and simulation results, Xu and coworkers (15) have further concluded that the breakdown and the associated fractional form are due to the two-state transformation related with the crossing of the Widom line when water undergoes supercooling.

All the above works identify the breakdown of the SE relation in supercooled water by monitoring the validity of the three variants without direct test of the original SE relation $D = k_B T / C \eta a$. This is questionable because the equivalence of the three variants to the original SE form is on the basis of various assumptions, while there are some evidences showing that those assumptions may not be valid all the time. For instance, a for organic molecules varies with volume fraction in their diluted solutions (3), and the behavior of ions in aqueous solutions is observed to deviate from the SE relation by taking a as a constant but the original SE relation actually holds if a is allowed to change (39-43). It is revealed that the variation of a is caused by the fact that molecules or ions in solutions move effectively with their surrounding shells. Another problem is the *ad hoc* choice of the first maximum of structure factor to calculate the structural relaxation time τ (15, 22, 34). The variant $D \sim \tau^{-1}$ is an exact result only when the displacements follow Gaussian or in the long-wavelength limit (34, 44), and the relation $\eta = G_\infty \tau$ is approximately established only when the memory effect is negligible (35). Besides, since supercooled water is a metastable liquid still in local equilibrium, the SE relation, as a form of the fluctuation-dissipation theorem, is believed to be valid (45). Furthermore, Shi and coworkers (32) have studied the three variants in softly repulsive and ortho-terphenyl systems and found that these variants

only give qualitatively consistent results but quantitatively deviate from each other as temperature decreases, and the deviations become larger at a lower temperature. All of the above studies indicate that, in supercooled water, the original SE relation may possibly still be valid while its variants are breakdown.

In this work, we perform MD simulations with the TIP5P and Jagla water models, respectively, to explore the consistency between the original SE relation and its variants in supercooled water. These two water models were previously adopted to explore the anomaly and the validity of the SE relation in supercooled water (15, 33, 46-48). Utilizing our simulation data, we first test the SE relation by $D \sim \tau^{-1}$, $D \sim T/\tau$, $D \sim T/\eta$, as well as the original form by $D \sim T/\alpha$, and then investigate the wavevector dependence of $D \sim \tau^{-1}$ and $D \sim T/\tau$. Our results indicate that the validity of $D \sim \tau^{-1}$ and $D \sim T/\tau$ depends on the specific choice of the wavevector value, and $D \sim \tau^{-1}$ is consistent with $D \sim T/\alpha$ only in the long-wavelength limit. Finally, the effective hydrodynamic radius a is calculated and related to the solvation effect. It is shown that a is not a constant, rather it decreases with decreasing temperature, which can be attributed to the solvation effect, namely the solvation shell structure and associated dynamics, so the variant $D \sim T/\eta$ may appear to be breakdown even if the original SE relation $D \sim T/\alpha$ holds.

2. Simulation details and analysis methods

2.1 Simulation details

In this work, we adopt the TIP5P and Jagla water models to perform our MD simulations since they have been previously used by others (15, 33) to observe the breakdown of SE variants and to show the anomaly of supercooled water. The initial configuration for the TIP5P model is consisted of 2048 molecules (49) with a constant density of 0.976 g/cm^3 , and that for the Jagla model (46-48) is consisted of 1728 molecules with a constant box size determined under a constant pressure $P = 153.33 \text{ bar}$ at each temperature. Although the reduced unit is usually adopted when using the Jagla model, we use the SI unit instead by assigning the unit of hardcore diameter $d = 0.3 \text{ nm}$, that of potential $U_0 = 100k_B$,

and that of pressure $P_0 = U_0 / d^3$. All our MD simulations were performed with the GROMACS MD simulation package (50, 51) and the periodic boundary conditions were applied in all three directions of the Cartesian space. The particle mesh Ewald algorithm (52) was employed to calculate the long-range electrostatic interactions with a cutoff of 1.2 nm in the real space and the van der Waals interactions were calculated directly with a truncated spherical cutoff of 1.2 nm for TIP5P and 1.0 nm for Jagla. Twenty-five temperatures simulated with the TIP5P model are distributed in the range of 240-390 K and twenty-four temperatures simulated with the Jagla model are in the range of 30-140 K. The system temperature was kept a constant by the Nosé-Hoover thermostat (53, 54) and the pressure was controlled by the Parrinello-Rahman barostat (55, 56). The simulation time step is 1 fs and the total simulated MD steps for each case are 10^6 – 10^8 for TIP5P and 10^5 – 10^7 for Jagla depending on the temperature.

2.2 Analysis methods

To examine the original SE relation and its three variants, we have to determine the diffusion constant D , structural relaxation time τ , shear viscosity η , and frictional coefficient α . The diffusion constant is calculated via its asymptotic relation with the mean square displacement

$$D = \lim_{t \rightarrow \infty} \frac{\langle |\mathbf{r}_i(t) - \mathbf{r}_i(0)|^2 \rangle}{6t} \quad (1)$$

where $\mathbf{r}_i(t)$ is the position of the i th particle at time t , and $\langle \rangle$ denotes time average. The calculated D values are plotted in Fig. S1.

The structural relaxation of water is described by the self-intermediate scattering function (34)

$$F_s(k, t) = \frac{1}{N} \sum_i^N \langle e^{ik[\mathbf{r}_i(t) - \mathbf{r}_i(0)]} \rangle \quad (2)$$

where N is the number of water molecules, wavevector k is usually chosen as the first maximum of the static structure factor, which is 24.5 nm^{-1} for the TIP5P model and 12.5 nm^{-1} for the Jagla model, respectively. The k values within 2.5 – 24.5 nm^{-1} with an interval of 2 nm^{-1} for the TIP5P model and 2.5 – 12.5 nm^{-1} with an interval of 1 nm^{-1} for the Jagla model are adopted to investigate the k dependence of the wavevector for $D \sim \tau^{-1}$ and $D \sim T/\tau$, respectively. The structural relaxation usually follows an

exponential relaxation in simple liquids and τ is determined by $F_s(k, \tau) = e^{-1}$. The calculated τ for various k values are plotted in Fig. S2.

The method proposed by Hess (57) was employed to determine the shear viscosity because of its reliability and fast convergence. In this method, an external force $a_x = A \cdot \cos(qz)$ is applied in the X direction, where A is the maximum of a_x and $q = 2\pi/l$ with l being the simulation box size, z the coordinate in the Z direction. The steady-state solution of the fluid equation is

$$u_x(z) = V(1 - e^{-t/\tau})\cos(qz) \quad (3)$$

where V is a constant which reflects the maximum value of $u_x(z)$ after reaching the non-equilibrium steady state. The shear viscosity is

$$\eta = A\rho/Vq^2 \quad (4)$$

Because density ρ and q are the same for the NVT ensemble with TIP5P at different temperatures, we use the ratio A/V to evaluate the shear viscosity given by TIP5P. By contrast, the viscosity given by the Jagla model is evaluated by $\eta \sim A/Vl$, which also takes into account the contribution from the temperature-dependent box size under a constant pressure. The calculated η are plotted in Fig. S3.

The frictional coefficient α is determined by applying a constant external force F_e on 128 selected molecules and all other particles are treated as the background media. In the linear response regime, the frictional force on an ion $f_r = \alpha v$ is equal to F_e after reaching the non-equilibrium steady state. The frictional coefficient $\alpha = C\eta v$ can thus be determined by

$$\alpha = \frac{F_e}{v} \quad (5)$$

where v can be calculated by $v = \lim_{t \rightarrow \infty} \frac{\langle r(t) \rangle}{t}$ (58). The calculated α is plotted in Fig. S4. Combining Eqs. (4) and (5), the hydrodynamic radius can be evaluated by $a \sim \alpha/\eta$.

The solvation effect can be described by the coordination number (average number of particles in the first solvation shell) and its lifetime. The coordination number (59) can be calculated by

$$n = \int_0^{r_c} g(r) 4\pi r^2 dr \quad (6)$$

where r_c is the position of the first minimum in the radial distribution function $g(r)$, which is 0.38 nm for TIP5P and 0.39 nm for Jagla. The residence time correlation function (58, 59) characterizing the lifetime of the first shell is defined by

$$C(t) = \langle \delta(0) \delta(t) \rangle \quad (7)$$

where $\delta(t)$ is 1 if a given molecule is still in the first solvation shell at time t and 0 otherwise. The residence correlation time τ_s can then be determined by the following relation:

$$C(\tau_s) = e^{-1} \quad (8)$$

3. Results

3.1 The validities of the original SE relation and its variants

To examine the original SE relation and its variants in supercooled water, we adopt the three formulas as $D \sim \tau^{-\xi_1}$, $D \sim (\tau/T)^{-\xi_2}$ and $D \sim (\eta/T)^{-\xi_3}$ to test the three variants, and take the formula $D \sim (\alpha/T)^{-\xi_4}$ to test the original SE relation. A variant or the original SE relation is valid if the corresponding exponent $\xi_i = 1.0$ ($i=1, 2, 3$ or 4), and invalid otherwise. The temperature dependences of D for TIP5P and Jagla, respectively, are plotted in Fig. S1 in Supporting Materials, and the temperature dependences of τ , η , and α are plotted in Figs. S2, S3, and S4, respectively. Based on these data, the logarithms of τ , τ/T (τ is calculated with the first maximum of static structure factor, which is $k = 24.5 \text{ nm}^{-1}$ for TIP5P and 12.5 nm^{-1} for Jagla), η/T , and α/T versus the logarithm of D for TIP5P are plotted in Fig. 1 and those for Jagla are plotted in Fig. 2.

It can be seen from Figs. 1a and 1b that the two variants $D \sim \tau^{-\xi_1}$ and $D \sim (\tau/T)^{-\xi_2}$ behave similarly for TIP5P: both ξ_1 and ξ_2 deviate significantly from 1.0, indicating the breakdown of these two variants. Each set of the data can be divided into two parts by a crossover temperature T_x , and each

part can be well fitted by a fractional form with a different ξ value. The T_x for $D \sim \tau^{-1}$ is around 285 K and 280 K for $D \sim T/\tau$, both with $\xi_1, \xi_2 < 1$ at $T < T_x$ and $\xi_1, \xi_2 > 1$ at $T > T_x$. Two fractional forms of $D \sim \tau^{-\xi_1}$ with $\xi_1 < 1$ are also observed in confined water on the fragile side and the strong side (19, 26). Xu and coworkers (15) have shown that $D \sim T/\tau$ is valid for a confined water at $T_x > 310$ K and for TIP5P at $T_x > 320$ K, but fractional forms with $\xi_2 < 1$ are observed for both systems at $T < T_x$. As shown in Fig. 1c, the variant $D \sim (\eta/T)^{-\xi_3}$ also follows two fractional forms with the crossover temperature located at $T_x \approx 280$ K, while the exponent $\xi_3 = 0.99$ manifests that $D \sim T/\eta$ is valid at $T > T_x$, and $\xi_3 = 0.82$ suggests its breakdown at $T < T_x$. This agrees with the experimental observation in water that $\xi_3 = 1$ at high temperatures and $\xi_3 = 0.8$ at low temperatures (18) as well as the simulation results with the TIP4P/2005 water model (17). In contrast to the implication of the breakdown of the SE relation by the above three variants, as shown in Fig. 1d, the fitted exponent $\xi_4 = 1.01$ for the whole simulated temperature range is so close to 1.0 that it strongly supports the validity of the original SE relation.

The simulation data with the Jagla model can also be well fitted by the two fractional forms of $D \sim \tau^{-\xi_1}$ and $D \sim (\tau/T)^{-\xi_2}$, as shown in Figs. 2a and 2b. The crossover temperature is $T_x \approx 43.3$ K for the former and $T_x \approx 37.0$ K for the latter. Both values of $\xi_1 = 0.88$ at $T < T_x$ and $\xi_1 = 1.86$ at $T > T_x$ manifest the breakdown of $D \sim \tau^{-1}$; $\xi_2 = 0.98$ at $T > T_x$ is close to 1.0, indicating the validity of $D \sim T/\tau$ within 37–140 K, while it is invalid at $T < T_x$ with $\xi_2 = 0.82$. These results agree with the previous simulation work with the Jagla model by Xu and coworkers (15), in which $\xi_2 = 1$ at $T > T_x$ and $\xi_2 = 0.87$ at $T < T_x$. Different from the results for TIP5P shown in Fig. 1c, the data shown in Fig. 2c can be well fitted by $D \sim (\eta/T)^{-\xi_3}$ with $\xi_3 = 0.91$ and no crossover is observed. The fitted $\xi_4 = 1.02$ in $D \sim (\alpha/T)^{-\xi_4}$ suggests that the original form $D \sim T/\alpha$ is valid for the Jagla

model.

Combining the results given by both TIP5P and Jagla, the validity of the original SE relation $D \sim T/\alpha$ is confirmed, even though at the same time all three variants $D \sim \tau^{-1}$, $D \sim T/\tau$, and $D \sim T/\eta$ are more or less breakdown in the whole simulated temperature ranges. Therefore, we conclude that the three variants are not good substitutes for inspecting the validity of the original SE relation in supercooled water.

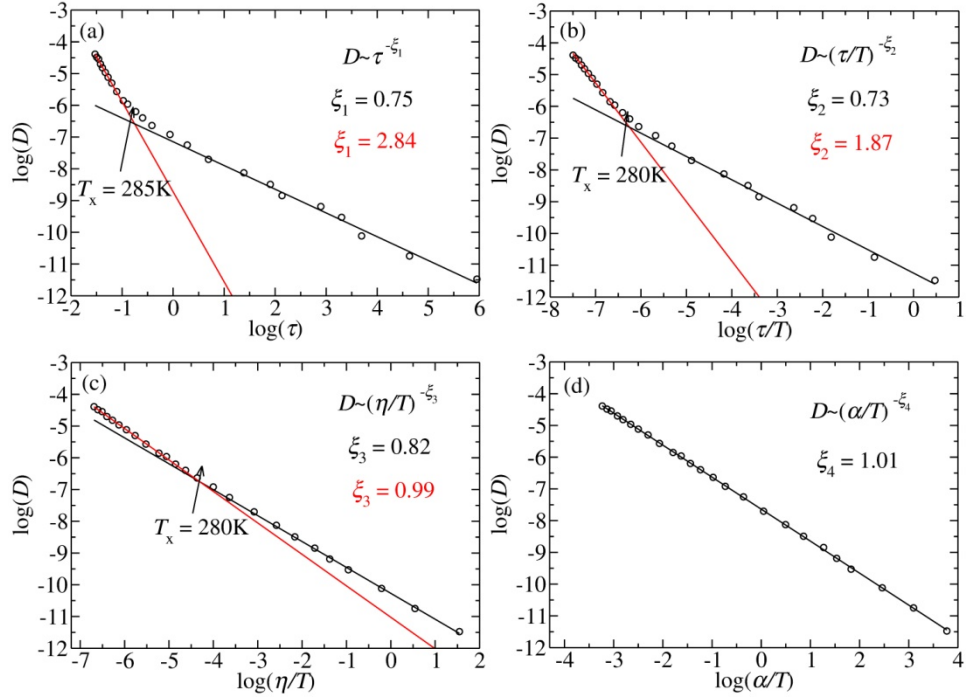


Fig. 1. Verification of the validities of the SE relation and its variants for the TIP5P water model: (a) $D \sim \tau^{-1}$; (b) $D \sim T/\tau$; (c) $D \sim T/\eta$; (d) $D \sim T/\alpha$. The calculated data are represented by circles and fitted by $D \sim \tau^{-\xi_1}$, $D \sim (\tau/T)^{-\xi_2}$, $D \sim (\eta/T)^{-\xi_3}$, and $D \sim (\alpha/T)^{-\xi_4}$, respectively. The fitted exponent ξ is written in the same color as the corresponding solid fitting line.

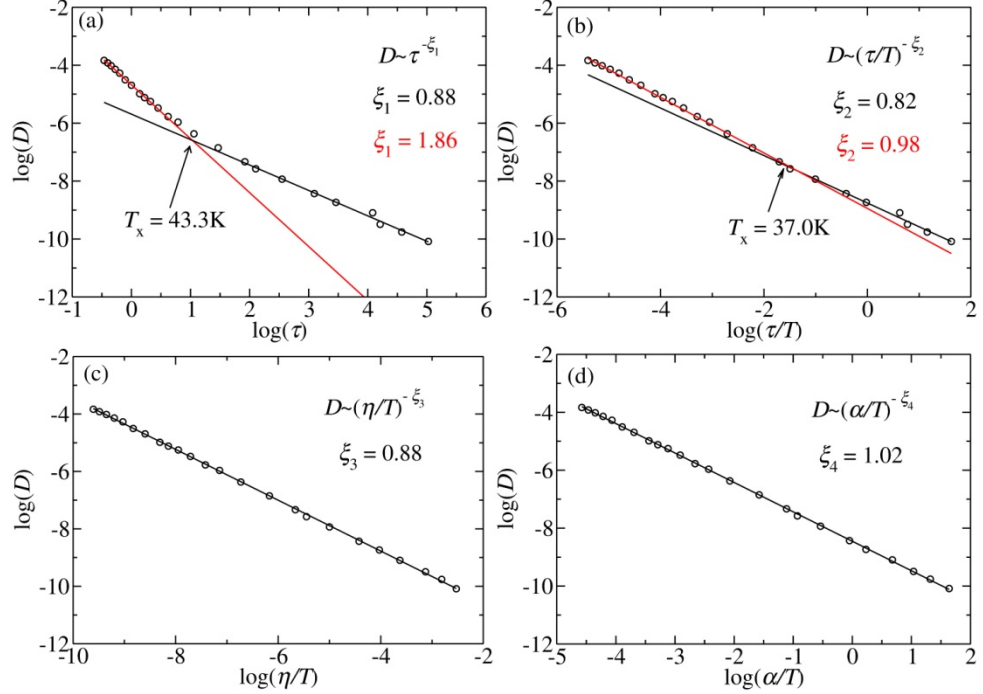


Fig. 2. Verification of the validities of the SE relation and its variants for the Jagla water model: (a) $D \sim \tau^{-1}$; (b) $D \sim T/\tau$; (c) $D \sim T/\eta$; (d) $D \sim T/\alpha$. The calculated data are represented by circles and fitted by $D \sim \tau^{-\xi_1}$, $D \sim (\tau/T)^{-\xi_2}$, $D \sim (\eta/T)^{-\xi_3}$, and $D \sim (\alpha/T)^{-\xi_4}$, respectively. The fitted exponent ξ is written in the same color as the corresponding solid fitting line.

3.2 The k dependence of the exponent in $D \sim \tau^{-\xi_1}$ and $D \sim (\tau/T)^{-\xi_2}$

The structural relaxation is usually quantified by choosing the wavevector k to be the first maximum of the static structure factor (15, 32, 34). However, there are no logical reasons one should make such a choice. On the contrary, there are some evidences showing that the structural relaxation depends on k (44), and thus the fitted exponents in $D \sim \tau^{-\xi_1}$ and $D \sim (\tau/T)^{-\xi_2}$ may also depend on k . The k -dependent $D \sim \tau^{-\xi_1}$ with three different k values for TIP5P and Jagla are plotted in Figs. 3a and 3b, respectively. Similar to the data shown in Figs. 1a and 2a, the data for both the TIP5P and Jagla models can be fitted by two $D \sim \tau^{-\xi_1}$ with a crossover temperature T_x , with one exponent $\xi_{1s} < 1$ at $T < T_x$ and the other $\xi_{1d} > 1$ at $T > T_x$. The exponent ξ_{1s} increases while ξ_{1d} decreases with decreasing k . Therefore, the variant $D \sim \tau^{-1}$ has different results with different k values, and it is exact only if the

particle displacement follows Gaussian (34). However, particle displacement does not follow Gaussian even in a system as simple as hard sphere because of the long-time tail effect (35, 60). Taking the long-time tail into account, the self-intermediate scattering function can be described by (44)

$$\ln F_s(k, t) = -Dk^2t + 3(2\gamma/\pi)^{1/2} Dk^2 (t\tau_c)^{1/2} + \dots \quad (9)$$

where $\gamma=1$ for pure liquid, $\tau_c = m/\alpha$ is the characteristic time for the Brownian motion, and m is the molecular mass. The first term at the right hand side corresponds to the Gaussian case, and the second term corresponds to the memory effect. The second term is usually smaller than the first term, but it does alter the structural relaxation time τ from the Gaussian case, and can be omitted only in the long-wavelength limit $k \rightarrow 0$. The exponents for different k values are plotted in Figs. 3c and 3d for TIP5P and Jagla models, respectively. The ξ_{ld} value decreases while ξ_{ls} increases with decreasing k , and both approach 1.0 as k decreases. The above result is consistent with Eq. (9) that $D \sim \tau^{-1}$ is exact only when $k \rightarrow 0$. Moreover, $D \sim \tau^{-1}$ is consistent to $D \sim T/\alpha$ when $k \rightarrow 0$.

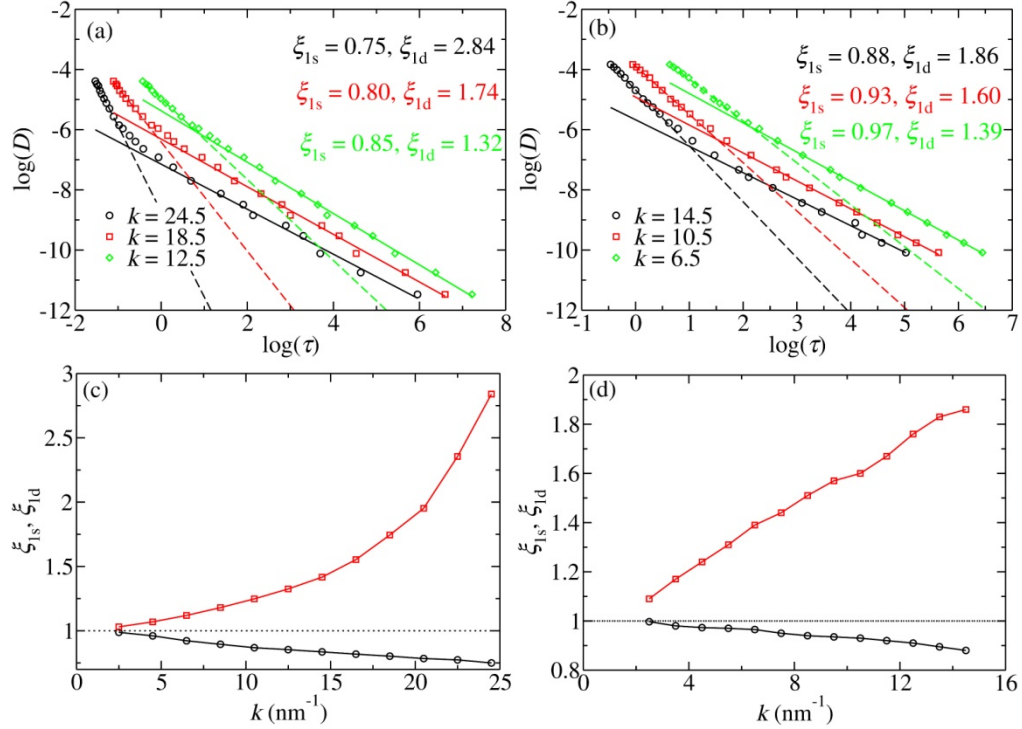


Fig. 3. Fitting of the k -dependent exponent ξ_l by $D \sim \tau^{-\xi_l}$ for TIP5P (a) and Jagla (b), as well as ξ_l

vs. k for TIP5P (c) and Jagla (d). In (a) and (b), the calculated data are represented by different symbols and the fitted exponent is written in the same color as the corresponding fitting line; ξ_{1s} values correspond to solid lines and ξ_{1d} values correspond to dotted lines. In (c) and (d), black circles represent ξ_{1s} and red squares are ξ_{1d} .

Because τ is k -dependent, the exponent ξ_2 in $D \sim (\tau/T)^{-\xi_2}$ should also be k -dependent. The ξ_2 values as a function of three different k values are plotted in Figs. 4a and 4b for TIP5P and Jagla, respectively, which demonstrates that ξ_2 is k -dependent for both TIP5P and Jagla. Similar to $D \sim \tau^{-\xi_1}$ shown in Fig. 3, the data can also be well fitted by two fractional forms with a crossover temperature. The exponents for different k values are plotted in Figs. 4c and 4d for TIP5P and Jagla, respectively. ξ_{2s} changes with temperature in a way similar to ξ_{1s} , but ξ_{2d} does not change in the same way as ξ_{1d} . At low temperatures, because τ is sensitive to T , ξ_{2s} approaches 1.0 as k decreases. By contrast, at high temperatures, τ is insensitive to T and T plays a more important role than τ in $D \sim (\tau/T)^{-\xi_2}$, so ξ_{2d} does not approach 1 even when $k \rightarrow 0$.

Combining the results given by ξ_{2s} and ξ_{2d} , we may conclude that there is a trend to approach 1.0 as $k \rightarrow 0$ for ξ_{2s} at low temperatures, but no such a trend is observed for ξ_{2d} at high temperatures, and thus the basic presumption $\eta = G_\infty \tau$ in $D \sim T/\tau$ is only an approximate relation (35). Although $D \sim T/\tau$ sometimes gives consistent results with $D \sim T/\alpha$ for a specific k at a certain temperature range, the results are k -dependent and not fulfilled for all data.

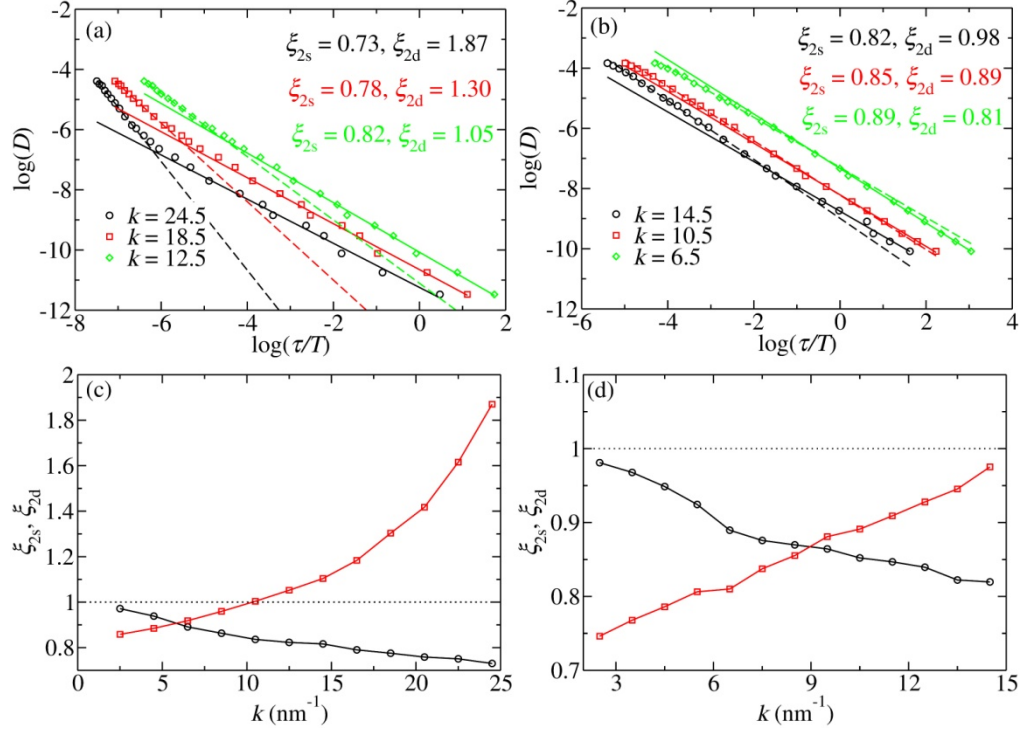


Fig. 4. Fitting of the k -dependent exponent ξ_2 by $D \sim (\tau/T)^{-\xi_2}$ for TIP5P (a) and Jagla (b) as well as ξ_2 vs. k for TIP5P (c) and Jagla (d). In (a) and (b), the calculated data are represented by different symbols and the fitted exponent is written in the same color as the corresponding fitting line, and ξ_{2s} values correspond to solid lines and ξ_{2d} values correspond to dotted lines. In (c) and (d), black circles represent ξ_{2s} and red squares are ξ_{2d} .

3.3 Variation of the effective hydrodynamic radius with thermal condition

The effective hydrodynamic radius is usually regarded as a constant when the three variants of the SE relation are employed. However, it was reported to change its value with different volume fractions or ions in diluted organic solution and aqueous ionic solution (3, 39-42). Therefore, the effective hydrodynamic radius in supercooled water may also change when the correlation between the central molecule and its surrounding shell increases as temperature decreases. In this work, the effective hydrodynamic radius is evaluated by $a \sim \alpha/\eta$, which is rescaled by its value at $T = 390$ K for the TIP5P model and by the value at $T = 140$ K for the Jagla model, respectively. The rescaled $\overline{\alpha/\eta}$ are plotted in

Fig. 5, demonstrating that $\overline{\alpha/\eta}$ for TIP5P is approximately a constant for $T > 280$ K but starts to decrease significantly when $T < 280$ K, and the change occurs at almost the same temperature as T_x observed in Figs. 1a and 1b. This result is consistent with $D \sim (\eta/T)^{-\xi_3}$ shown in Fig. 1c and similar to the previous observations (17, 18, 26, 37). For the Jagla model, $\overline{\alpha/\eta}$ monotonically decreases during cooling, and the decreasing rate is small when $T > 45$ K but becomes larger when $T < 45$ K. Again, the transition temperature is close to T_x for the two variants $D \sim \tau^{-1}$ and $D \sim T/\tau$ shown in Figs. 2a and 2b.

The trend of a changing with temperature can be understood as follows. A water molecule drags the effective shells composed of surrounding water molecules to move together. Here we only consider water molecules in the first coordination shell which play the most important role (43) and form a composite particle along with the central water molecule. The interaction between the central molecule and its first solvation shell is different under different conditions, which can be described by the coordination number n and the residence correlation time τ_s . A larger τ_s corresponds to a larger probability for molecules in the first shell to move together with the central molecule. The average number of water molecules in the composite particle is $1 + np(\tau_s)$, where 1 denotes the central molecule and p is the probability of the first shell moving with the central molecule, which increases monotonically with τ_s . By assuming both free molecules and the composite particle are spheres, the effective hydrodynamic radius of the composite particle is roughly $[1 + np(\tau_s)]^{1/3} a_0$, where a_0 is the effective hydrodynamic radius of a free molecule. Because the frictional force applied to the composite particle $\sim C\eta v [1 + np(\tau_s)]^{1/3} a_0$ should be equal to the sum of the frictional force applied to each molecule in the composited particle $\sim C\eta v [1 + np(\tau_s)] a$, where v is the velocity of the composite particle, the average effective hydrodynamic radius a of a molecule can be described by

$$a \sim \frac{a_0}{[1 + np(\tau_s)]^{2/3}} \quad (10)$$

The coordination number n of the first shell and the residence correlation time τ_s calculated according to our simulation data are plotted in Fig. 6. For the TIP5P model, as shown in Figs. 6a and 6c, when temperature decreases, n decreases because of the more ordered structure of water (15, 61, 62), while τ_s increases because the coupling between molecules becomes stronger. At high temperatures, these two factors contribute oppositely to $np(\tau_s)$ and almost cancel with each other, so the change of a is approximately a constant. At low temperatures, the increases of τ_s is much faster than n decreases, so $p(\tau_s)$ plays a more significant role than n , leading to the decrease of a . For the Jagla model, as shown in Figs. 6b and 6d, as temperature decreases, both n and τ_s contribute to the increase of $np(\tau_s)$, leading to monotonically decrease of a with decreasing temperature. The decrease of $a \sim T/D\eta$ with decreasing temperature in supercooled water has also been observed in previous works, indicated either by the decrease of $D\eta/T$ with increasing temperature (26, 63) or by $D \sim (\eta/T)^{-\xi_3}$ with $\xi_3 < 1$ (17, 18, 23). The decrease of a with decreasing temperature is also observed in other liquids, such as supercooled binary Lennard-Jones liquids (25, 64), supercooled aqueous solutions of glycerol (14), water/methanol solutions (24), ortho-terphenyl (32, 65), and tris-Naphthylbenzene (20). Therefore, we conclude that a may indeed vary with thermal condition, which should be considered while testing the SE relation.

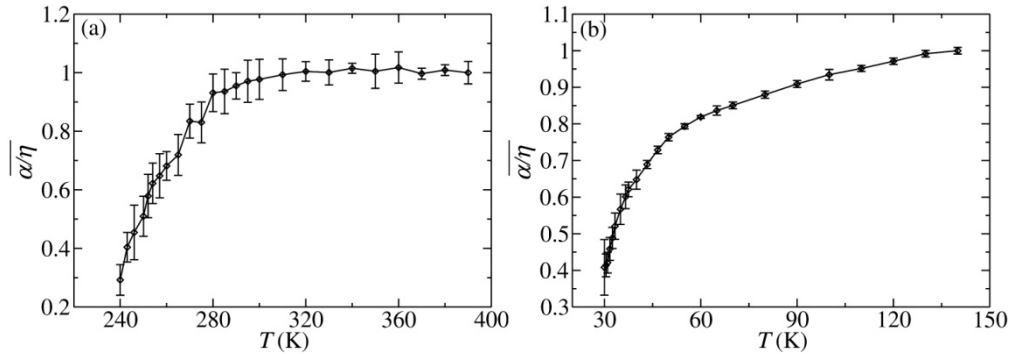


Fig. 5. Rescaled effective hydrodynamic radius $\overline{\alpha/\eta}$ vs. T for the TIP5P model (a) and the Jagla model (b).

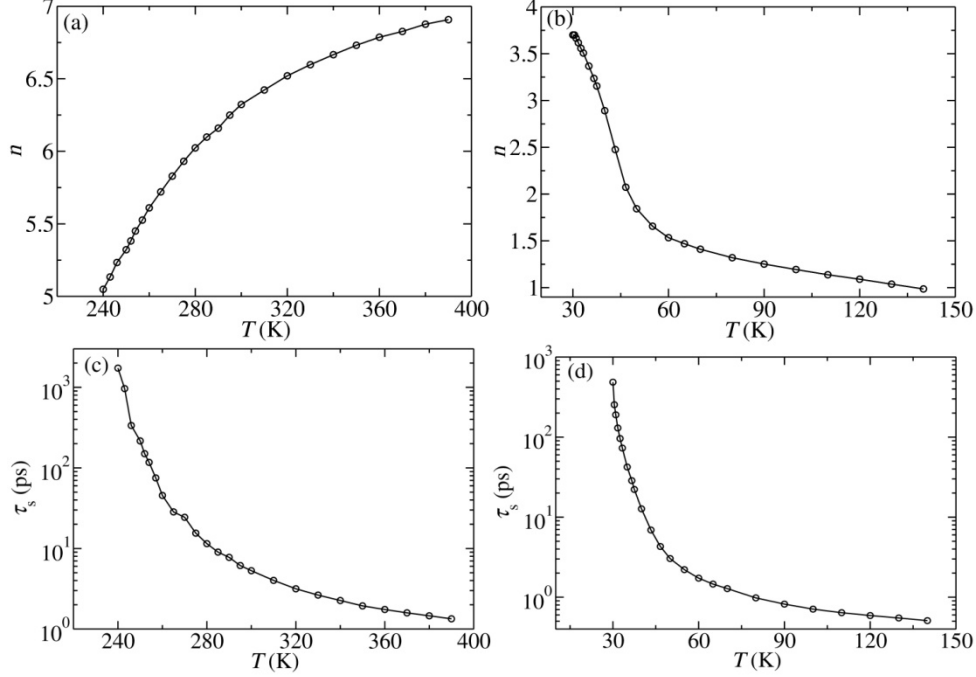


Fig. 6. Coordination number n vs. T for the TIP5P model (a) and the Jagla model (b), and the residence correlation time τ_s of the first solvation shell vs. T for the TIP5P model (c) and the Jagla model (d).

4. Conclusion and Discussion

In this work, we perform atomistic MD simulations to explore the validity of the SE relation in supercooled water with the TIP5P model in the range of 230–390 K and the Jagla model in the range of 30–140 K. Our results confirm the validity of the original SE relation $D = k_B T / C \eta a$ in supercooled water, even though its three variants, $D \sim \tau^{-1}$, $D \sim T/\tau$ and $D \sim T/\eta$, are all breakdown and in their fractional forms. The two variants, $D \sim \tau^{-1}$ and $D \sim T/\tau$, follow fractional forms like $D \sim \tau^{-\xi_1}$ and $D \sim (\tau/T)^{-\xi_2}$ with a crossover temperature T_x , which is around 280 K for the TIP5P model and 40 K for the Jagla model. Both exponents ξ_1 and ξ_2 are different on the two sides of T_x and is k -dependent. The variant $D \sim \tau^{-1}$ agrees with $D \sim T/\alpha$ only in the long-wavelength limit, and the variant $D \sim T/\tau$ is an approximate formula, which agrees with $D \sim T/\alpha$ only when a specific k is chosen in a certain temperature range. The variant $D \sim T/\eta$ gives rational results only when the effective hydrodynamic

radius a can be considered as a constant. Moreover, although the three variants give similar qualitative results, the exponents are different from each other, so the structural relaxation times τ and τ/T are not good substitutes of viscosity η . Consequently, the three variants are usually not good variants of the SE relation, which should be critically and quantitatively evaluated while they are used to test the validity of the SE relation.

We have also found that the effective hydrodynamic radius a changes with thermal condition. It is almost a constant in the range of 280-390 K for the TIP5P model and decreases with decreasing temperature at $T < 280$ K, while it monotonically decreases with decreasing temperature for the Jagla model. The change of a for the TIP5P model results from the competition between the decrease of the coordination number in the first coordination shell and the increase of the residence correlation time with decreasing temperature. By contrast, both the coordination number and the residence correlation time for the Jagla model increase with decreasing temperature, which allows more water molecules to move with the central water molecule and thus a decreases with decreasing temperature. Our results emphasize the importance of considering the change of a when investigating the validity of the SE relation in supercooled water. By looking into the breakdown of the variants of the SE relation, it is very likely that our conclusion is universal and should hold for other supercooled liquids.

The temperature ranges of our MD simulations are limited to 230-390 K for TIP5P and 30-140 K for Jagla, respectively, because large fluctuations out of them disallow accurate determination of viscosity and frictional coefficient with the current simulation scale and computational precision. Our future work could be, by employing more computer resources, extending our simulations to low temperatures to see at which temperature the original SE relation will eventually break down, and how the scaling of τ and D will differ.

Acknowledgments:

The authors thank Prof. Fanlong Meng for his critical reading of this paper. This work was supported by the Strategic Priority Research Program of Chinese Academy of Sciences (Grant No. XDA17010504), the National Natural Science Foundation of China (Nos. 11774357, 12047503) and the Science Foundation of

Civil Aviation Flight University of China (Nos. J2019-059, JG2019-19). The allocation of computer time on the HPC cluster of ITP-CAS is also appreciated.

Supplementary Figures

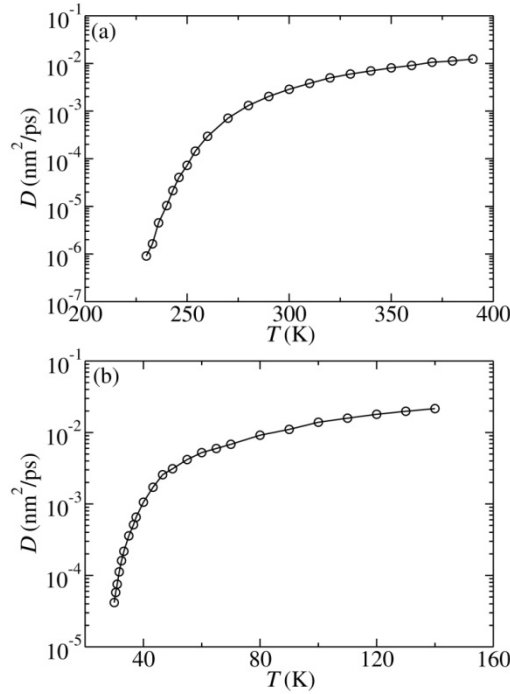


Fig. S1. The diffusion constant D as a function of temperature T : (a) TIP5P; (b) Jagla.

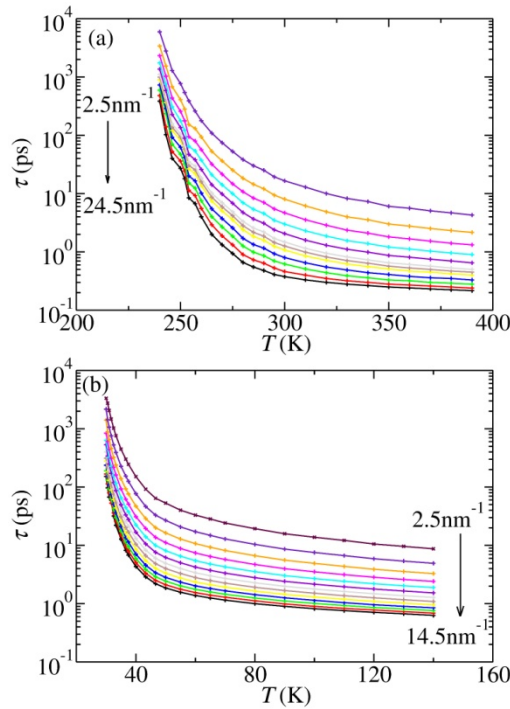


Fig. S2. The structural relaxation time τ for various wavevector k as a function of temperature T : (a) TIP5P; (b) Jagla.

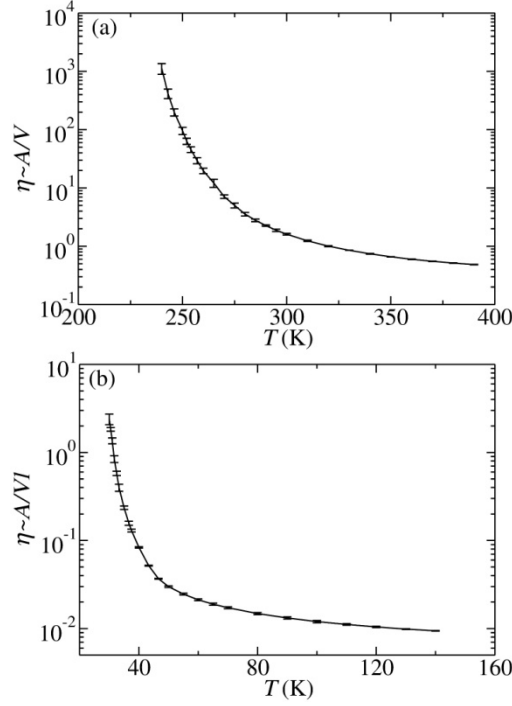


Fig. S3. The viscosity η as a function of temperature T :(a) TIP5P; (b) Jagla.

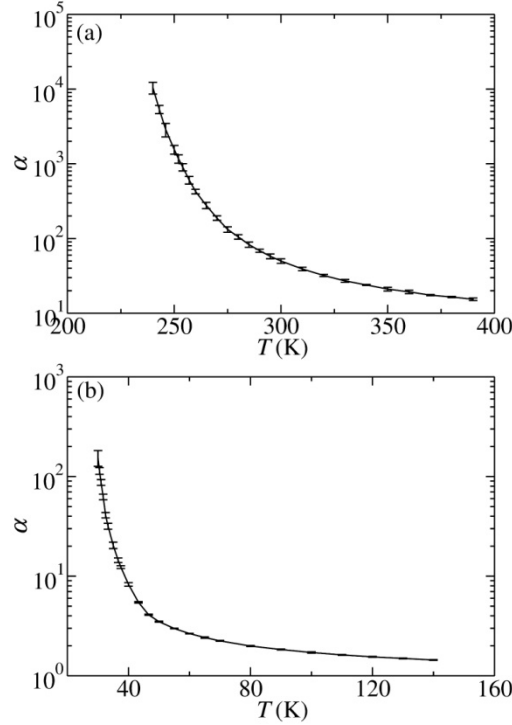


Fig. S4. The frictional coefficient α as a function of temperature T :(a) TIP5P; (b) Jagla.

References

1. L. D. Landau, E. M. Lifshitz, *Fluid Mechanics*. (Pergamon, Oxford, 1987).

2. M. E. Young, P. A. Carroad, R. L. Bell, Estimation of diffusion coefficients of proteins. *Biotechnol. Bioeng.* **22**, 947-955 (1980).
3. S. G. Schultz, A. K. Solomon, Determination of the Effective Hydrodynamic Radii of Small Molecules by Viscometry. *The Journal of General Physiology* **44**, 1189-1199 (1961).
4. M. R. McCarthy, K. D. Vandegriff, R. M. Winslow, The role of facilitated diffusion in oxygen transport by cell-free hemoglobins: implications for the design of hemoglobin-based oxygen carriers. *Biophys. Chem.* **92**, 103-117 (2001).
5. P. A. Gordon, Extrapolation of Rheological Properties for Lubricant Components with Stokes–Einstein Relationships. *Industrial & Engineering Chemistry Research* **44**, 5828-5835 (2005).
6. S. Gupta, J. Stellbrink, E. Zaccarelli, C. N. Likos, M. Camargo, P. Holmqvist, J. Allgaier, L. Willner, D. Richter, Validity of the Stokes-Einstein Relation in Soft Colloids up to the Glass Transition. *Phys. Rev. Lett.* **115**, 128302 (2015).
7. D. Bonn, W. K. Kegel, Stokes–Einstein relations and the fluctuation-dissipation theorem in a supercooled colloidal fluid. *J. Chem. Phys.* **118**, 2005-2009 (2003).
8. C. Comminges, R. Barhdadi, M. Laurent, M. Troupel, Determination of Viscosity, Ionic Conductivity, and Diffusion Coefficients in Some Binary Systems: Ionic Liquids + Molecular Solvents. *Journal of Chemical & Engineering Data* **51**, 680-685 (2006).
9. A. Noda, K. Hayamizu, M. Watanabe, Pulsed-Gradient Spin–Echo ¹H and ¹⁹F NMR Ionic Diffusion Coefficient, Viscosity, and Ionic Conductivity of Non-Chloroaluminate Room-Temperature Ionic Liquids. *J. Phys. Chem. B* **105**, 4603-4610 (2001).
10. B. T. Poe, P. F. McMillan, D. C. Rubie, S. Chakraborty, J. Yarger, J. Diefenbacher, Silicon and Oxygen Self-Diffusivities in Silicate Liquids Measured to 15 Gigapascals and 2800 Kelvin. *Science* **276**, 1245-1248 (1997).
11. E. D. Snijder, M. J. M. te Riele, G. F. Versteeg, W. P. M. van Swaaij, Diffusion coefficients of several aqueous alkanolamine solutions. *Journal of Chemical & Engineering Data* **38**, 475-480 (1993).
12. M. Terazima, K. Okamoto, N. Hirota, Diffusion process of methyl red in organic solvents studied by the transient grating method. *The Journal of Physical Chemistry* **97**, 5188-5192 (1993).
13. J. Świergiel, I. Płowaś, J. Jadżyn, Charge Relaxation and Stokes–Einstein Relation in Diluted Electrolyte Solution of Propylene Carbonate and Lithium Perchlorate. *Industrial & Engineering Chemistry Research* **54**, 2108-2113 (2015).
14. B. Chen, E. E. Sigmund, W. P. Halperin, Stokes-Einstein Relation in Supercooled Aqueous Solutions of Glycerol. *Phys. Rev. Lett.* **96**, 145502 (2006).
15. L. Xu, F. Mallamace, Z. Yan, F. W. Starr, S. V. Buldyrev, H. Eugene Stanley, Appearance of a fractional Stokes-Einstein relation in water and a structural interpretation of its onset. *Nat Phys* **5**, 565-569 (2009).
16. M. G. Mazza, N. Giovambattista, H. E. Stanley, F. W. Starr, Connection of translational and rotational dynamical heterogeneities with the breakdown of the Stokes-Einstein and Stokes-Einstein-Debye relations in water. *Phys. Rev. E* **76**, 031203 (2007).

17. T. Kawasaki, K. Kim, Identifying time scales for violation/preservation of Stokes-Einstein relation in supercooled water. *Science Advances* **3**, e1700399 (2017).
18. A. Dehaoui, B. Issenmann, F. Caupin, Viscosity of deeply supercooled water and its coupling to molecular diffusion. *Proc. Natl. Acad. Sci. U. S. A.* **112**, 12020-12025 (2015).
19. S. H. Chen, F. Mallamace, C. Y. Mou, M. Broccio, C. Corsaro, A. Faraone, L. Liu, The violation of the Stokes-Einstein relation in supercooled water. *Proc Natl Acad Sci U S A* **103**, 12974-12978 (2006).
20. S. F. Swallen, P. A. Bonvallet, R. J. McMahon, M. D. Ediger, Self-Diffusion of tris-Naphthylbenzene near the Glass Transition Temperature. *Phys. Rev. Lett.* **90**, 015901 (2003).
21. J. Habasaki, C. Leon, K. Ngai, *Dynamics of glassy, crystalline and liquid ionic conductors*. Top Appl Phys (Springer, Berlin, 2017), vol. 132.
22. D. Jeong, M. Y. Choi, H. J. Kim, Y. Jung, Fragility, Stokes-Einstein violation, and correlated local excitations in a coarse-grained model of an ionic liquid. *Phys. Chem. Chem. Phys.* **12**, 2001-2010 (2010).
23. I. N. Tsimpanogiannis, S. H. Jamali, I. G. Economou, T. J. H. Vlugt, O. A. Moulton, On the validity of the Stokes–Einstein relation for various water force fields. *Mol. Phys.*, 1-11 (2019).
24. C. Corsaro, E. Fazio, D. Mallamace, The Stokes-Einstein relation in water/methanol solutions. *J. Chem. Phys.* **150**, 234506 (2019).
25. P. Bordat, F. d. r. Affouard, M. Descamps, F. M. ller-Plathe, The breakdown of the Stokes–Einstein relation in supercooled binary liquids. *J. Phys.: Condens. Matter* **15**, 5397-5407 (2003).
26. F. Mallamace, C. Branca, C. Corsaro, N. Leone, J. Spooren, H. E. Stanley, S.-H. Chen, Dynamical Crossover and Breakdown of the Stokes–Einstein Relation in Confined Water and in Methanol-Diluted Bulk Water. *J. Phys. Chem. B* **114**, 1870-1878 (2010).
27. L. O. Hedges, L. Maibaum, D. Chandler, J. P. Garrahan, Decoupling of exchange and persistence times in atomistic models of glass formers. *J. Chem. Phys.* **127**, 211101 (2007).
28. Y. Jung, J. P. Garrahan, D. Chandler, Dynamical exchanges in facilitated models of supercooled liquids. *J. Chem. Phys.* **123**, 084509 (2005).
29. Y. Jung, J. P. Garrahan, D. Chandler, Excitation lines and the breakdown of Stokes-Einstein relations in supercooled liquids. *Phys. Rev. E* **69**, 061205-061205 (2004).
30. S. Sengupta, S. Karmakar, C. Dasgupta, S. Sastry, Breakdown of the Stokes-Einstein relation in two, three, and four dimensions. *J. Chem. Phys.* **138**, 12A548 (2013).
31. O. Blondel, C. Toninelli, Is there a fractional breakdown of the Stokes-Einstein relation in kinetically constrained models at low temperature? *EPL (Europhysics Letters)* **107**, 26005 (2014).
32. Z. Shi, P. G. Debenedetti, F. H. Stillinger, Relaxation processes in liquids: Variations on a theme by Stokes and Einstein. *J. Chem. Phys.* **138**, 12A526 (2013).
33. P. Kumar, S. V. Buldyrev, S. R. Becker, P. H. Poole, F. W. Starr, H. E. Stanley, Relation between the Widom line and the breakdown of the Stokes–Einstein relation in supercooled water. *Proc. Natl. Acad. Sci. U. S. A.* **104**, 9575-9579 (2007).

34. K. Binder, W. Kob, *Glassy materials and disordered solids: An introduction to their statistical mechanics*. (World Scientific, 2011).
35. J. Barrat, J. Hansen, *Basic concepts for simple and complex liquids*. (Cambridge University Press, Cambridge, 2003).
36. V. Dubey, S. Erimban, S. Indra, S. Daschakraborty, Understanding the Origin of the Breakdown of the Stokes–Einstein Relation in Supercooled Water at Different Temperature–Pressure Conditions. *J. Phys. Chem. B* **123**, 10089-10099 (2019).
37. E. Guillaud, S. Merabia, D. de Ligny, L. Joly, Decoupling of viscosity and relaxation processes in supercooled water: a molecular dynamics study with the TIP4P/2005f model. *Phys. Chem. Chem. Phys.* **19**, 2124-2130 (2017).
38. F. Mallamace, M. Broccio, C. Corsaro, A. Faraone, L. Liu, C.-Y. Mou, S.-H. Chen, Dynamical properties of confined supercooled water: an NMR study. *J. Phys.: Condens. Matter* **18**, S2285-S2297 (2006).
39. S. H. Lee, J. C. Rasaiah, Molecular dynamics simulation of ionic mobility. I. Alkali metal cations in water at 25° C. *J. Chem. Phys.* **101**, 6964-6974 (1994).
40. S. H. Lee, J. C. Rasaiah, Molecular dynamics simulation of ion mobility. 2. Alkali metal and halide ions using the SPC/E model for water at 25 C. *The Journal of Physical Chemistry* **100**, 1420-1425 (1996).
41. G. Ren, L. Chen, Y. Wang, Dynamic heterogeneity in aqueous ionic solutions. *Phys. Chem. Chem. Phys.* **20**, 21313-21324 (2018).
42. J. Hubbard, L. Onsager, Dielectric dispersion and dielectric friction in electrolyte solutions. I. *J. Chem. Phys.* **67**, 4850-4857 (1977).
43. L. M. Varela, M. García, V. c. Mosquera, Exact mean-field theory of ionic solutions: non-Debye screening. *Phys. Rep.* **382**, 1-111 (2003).
44. J. P. Boon, S. Yip, *Molecular hydrodynamics*. (Courier Corporation, 1991).
45. P. G. Debenedetti, *Metastable liquids: concepts and principles*. (Princeton University Press, Princeton, 1996).
46. E. A. Jagla, A model for the fragile-to-strong transition in water. *J. Phys.: Condens. Matter* **11**, 10251-10258 (1999).
47. E. A. Jagla, Low-temperature behavior of core-softened models: water and silica behavior. *Phys Rev E Stat Nonlin Soft Matter Phys* **63**, 061509 (2001).
48. E. A. Jagla, Core-softened potentials and the anomalous properties of water. *J. Chem. Phys.* **111**, 8980-8986 (1999).
49. M. W. Mahoney, W. L. Jorgensen, A five-site model for liquid water and the reproduction of the density anomaly by rigid, nonpolarizable potential functions. *J. Chem. Phys.* **112**, 8910-8922 (2000).
50. H. J. C. Berendsen, D. van der Spoel, R. van Drunen, GROMACS: A message-passing parallel molecular dynamics implementation. *Comput. Phys. Commun.* **91**, 43-56 (1995).
51. D. Van Der Spoel, E. Lindahl, B. Hess, G. Groenhof, A. E. Mark, H. J. Berendsen, GROMACS: fast, flexible, and free. *J. Comput. Chem.* **26**, 1701-1718 (2005).

52. U. Essmann, L. Perera, M. L. Berkowitz, T. Darden, H. Lee, L. G. Pedersen, A smooth particle mesh Ewald method. *J. Chem. Phys.* **103**, 8577-8593 (1995).
53. S. Nosé, A unified formulation of the constant temperature molecular dynamics methods. *J. Chem. Phys.* **81**, 511-519 (1984).
54. W. G. Hoover, Canonical dynamics: Equilibrium phase-space distributions. *Phys. Rev. A* **31**, 1695-1697 (1985).
55. M. Parrinello, A. Rahman, Polymorphic transitions in single crystals: A new molecular dynamics method. *J. Appl. Phys.* **52**, 7182-7190 (1981).
56. S. Nosé, M. L. Klein, Constant pressure molecular dynamics for molecular systems. *Mol. Phys.* **50**, 1055-1076 (1983).
57. B. Hess, Determining the shear viscosity of model liquids from molecular dynamics simulations. *J. Chem. Phys.* **116**, 209-217 (2002).
58. R. Shi, Y. Wang, Ion-Cage Interpretation for the Structural and Dynamic Changes of Ionic Liquids under an External Electric Field. *J. Phys. Chem. B* **117**, 5102-5112 (2013).
59. S. Koneshan, J. C. Rasaiah, R. Lynden-Bell, S. Lee, Solvent structure, dynamics, and ion mobility in aqueous solutions at 25 C. *J. Phys. Chem. B* **102**, 4193-4204 (1998).
60. B. J. Alder, T. E. Wainwright, Velocity Autocorrelations for Hard Spheres. *Phys. Rev. Lett.* **18**, 988-990 (1967).
61. R. Shi, J. Russo, H. Tanaka, Origin of the emergent fragile-to-strong transition in supercooled water. *Proc. Natl. Acad. Sci. U. S. A.* **115**, 9444-9449 (2018).
62. R. Ludwig, The Puzzling Properties of Supercooled and Glassy Water. *Angew. Chem. Int. Ed.* **45**, 3402-3405 (2006).
63. X.-J. H. Chen-Hui Li , Ying-Wei Luan, Jian-Guo Li, Abnormal breakdown of Stokes-Einstein relation in liquid aluminium. *Chin. Phys. B* **26**, 16102-016102 (2017).
64. F. Affouard, M. Descamps, L.-C. Valdes, J. Habasaki, P. Bordat, K. L. Ngai, Breakdown of the Stokes–Einstein relation in Lennard-Jones glassforming mixtures with different interaction potential. *J. Chem. Phys.* **131**, 104510 (2009).
65. M. K. Mapes, S. F. Swallen, M. D. Ediger, Self-Diffusion of Supercooled o-Terphenyl near the Glass Transition Temperature. *J. Phys. Chem. B* **110**, 507-511 (2006).